



## Open Archive TOULOUSE Archive Ouverte (OATAO)

OATAO is an open access repository that collects the work of Toulouse researchers and makes it freely available over the web where possible.

This is an author-deposited version published in : <http://oatao.univ-toulouse.fr/>  
Eprints ID : 9367

**To link to this article** : DOI:10.1016/j.electacta.2012.07.134  
URL : <http://dx.doi.org/10.1016/j.electacta.2012.07.134>

**To cite this version :**

Mesguich, David and Bassat, Jean-Marc and Aymonier, Cyril and Brüll, Annelise and Dessemond, Laurent and Djurado, Elisabeth  
*Influence of crystallinity and particle size on the electrochemical properties of spray pyrolyzed Nd<sub>2</sub>NiO<sub>4+δ</sub> powders.* (2013)  
Electrochimica Acta, vol. 87 . pp. 330-335. ISSN 0013-4686

Any correspondance concerning this service should be sent to the repository administrator: [staff-oatao@listes-diff.inp-toulouse.fr](mailto:staff-oatao@listes-diff.inp-toulouse.fr)

# Influence of crystallinity and particle size on the electrochemical properties of spray pyrolyzed $\text{Nd}_2\text{NiO}_{4+\delta}$ powders

D. Mesguich<sup>a,1</sup>, J.-M. Bassat<sup>a</sup>, C. Aymonier<sup>a</sup>, A. Brüll<sup>a</sup>, L. Dessemond<sup>b</sup>, E. Djurado<sup>b,\*</sup>

<sup>a</sup> CNRS, Université de Bordeaux, ICMCB, 87 avenue du Dr. A. Schweitzer, 33608 Pessac, France

<sup>b</sup> LEPMI, UMR 5279, CNRS, Grenoble INP, Université de Savoie, Université Joseph Fourier, BP75, 38402 Saint Martin d'Hères Cedex, France

## A B S T R A C T

This paper is dedicated to the study of the relationship between the  $\text{Nd}_2\text{NiO}_{4+\delta}$  powder micro-structural properties (especially particle size and crystallinity) and electrochemical properties when the oxide is used as SOFC cathode deposited on 8YSZ electrolyte coated with thin doped ceria. Nano-structured particles of  $\text{Nd}_2\text{NiO}_{4+\delta}$  with controlled crystallinity, size and morphology have been synthesized using ultrasonic spray pyrolysis (USP). The series and polarization resistances measured on symmetrical half cells  $\text{Nd}_2\text{NiO}_{4+\delta}/\text{YDC}/8\text{YSZ}/\text{YDC}/\text{Nd}_2\text{NiO}_{4+\delta}$  are both found to be dependent on the cathode microstructure and present a similar evolution with temperature. The best results are obtained for highly crystalline cathode powders combined with a small particle size.

## Keywords:

Solid oxide fuel cell

Cathode

Mixed ionic and electronic conductor

Electrochemical impedance spectroscopy

Nickelates

Ultrasonic spray pyrolysis

## 1. Introduction

Among the essential efforts devoted to SOFCs development, one of the long-established pathways deals with the cathode material optimization. The challenge is to obtain high activity for electrochemical oxygen reduction in the 600–700 °C temperature operating range while retaining chemical compatibility with electrolyte materials.

Rare-earth nickelates with the  $\text{K}_2\text{NiF}_4$ -type structure, namely  $\text{Ln}_2\text{NiO}_{4+\delta}$  ( $\text{Ln} = \text{La}, \text{Nd}, \text{Pr}$ ) appear to be promising materials for applications such as cathodes for low-temperature solid oxide fuel cells (LT-SOFCs) and oxygen separation membranes. In the past fifteen years, several groups have focused their researches on the development of these oxides [1–6]. The  $\text{A}_2\text{MO}_{4+\delta}$  structure, which consists of  $\text{MO}_6$  octahedra sheets interleaved by  $\text{A}_2\text{O}_2$  layers, shows alternative transport properties in comparison with those of the isotropic perovskite structure. Indeed, the anisotropy of anionic conductivity in this two dimensional-type structure was demonstrated on  $\text{La}_2\text{NiO}_{4+\delta}$  single crystals and thin films [7,8], the diffusion being at least one to two orders of magnitude higher in the (a, b) plane when compared with the perpendicular direction. The nickelate structure provides preferential path for oxygen

which results in high oxygen mobility. Moreover, such oxides are good electronic conductors thanks to the mixed valency of nickel ( $\text{Ni}^{2+}/\text{Ni}^{3+}$ ). Referred to as mixed ionic and electronic conductors (MIEC), these materials are highly desirable for improving the oxygen reduction kinetics. Indeed for high ionic and electrical conductivity the oxygen reduction reaction is likely to be delocalized over the whole electrode surface.

While current investigations on nickelates mainly focus on  $\text{La}_2\text{NiO}_{4+\delta}$  [9],  $\text{Nd}_2\text{NiO}_{4+\delta}$  was selected in this work because it shows a large over-stoichiometry in the whole temperature range 0–1000 °C [1,2] (for example  $\delta = 0.17$  at 700 °C), which should lead to improved properties. At 700 °C, its ionic conductivity is about  $0.01 \text{ S cm}^{-1}$  and its electronic conductivity is  $100 \text{ S cm}^{-1}$ . Its thermal expansion coefficient ( $\alpha = 12 \times 10^{-6} \text{ K}^{-1}$ ) makes this material compatible with usual electrolytes YSZ and doped ceria [1,2]. The electrocatalytic properties (surface exchange coefficient  $k = 10^{-6} \text{ cm s}^{-1}$  at 800 °C) and oxygen transport properties (oxygen diffusion coefficient  $D^* = 10^{-7} \text{ cm}^2 \text{ s}^{-1}$  at 800 °C) of  $\text{Nd}_2\text{NiO}_{4+\delta}$  surpass the best values obtained for references perovskite materials by about one order of magnitude, especially at moderate temperatures [1,2]. Moreover, the activation energy value for the oxygen diffusion (0.85 eV) is lower than in YSZ or perovskite materials such as LSF [10].

Electrochemical properties of nickelate materials have been previously reported,  $\text{Nd}_2\text{NiO}_{4+\delta}$  exhibits low ASR values (less than  $0.5 \Omega \text{ cm}^2$  at 700 °C), high current density (at 0.70 V,  $0.54 \text{ A cm}^{-2}$  at 700 °C) combined with a low reactivity with YSZ [11–14]. Here, the authors have explored an original route, namely ultrasonic

\* Corresponding author. Tel.: +33 0476826684; fax: +33 0476826777.

E-mail address: elisabeth.djurado@lepmi.grenoble-inp.fr (E. Djurado).

<sup>1</sup> Permanent address: Université de Toulouse, UPS, INP, Institut Carnot Cirimat, 118 route de Narbonne, F31062 Toulouse cedex 9, France.

spray pyrolysis (USP), to synthesize nanostructured cathode powders which could lead to improved electrochemical properties. USP is a technique relying on the ultrasonic atomization of a precursor solution to generate an aerosol subsequently pyrolyzed in a very short time. The main advantage of this technique is conferred by the droplets of the aerosol acting as individual micro-reactors, leading to micron and submicron powders. This method allows the synthesis of complex oxides submicron powders with very short reaction times: 1–10 s; the oxides produced are composed of nanocrystalline particles, generally eliminating the need for post-treatments.

This paper is dedicated to the study of the electrochemical properties of  $\text{Nd}_2\text{NiO}_{4+\delta}$  powders prepared by USP, when the oxide is used as cathode, deposited on 8YSZ electrolyte coated with thin doped ceria. The addition of such thin ionic conducting interface between 8YSZ and the cathode layer, also acting as a buffer layer, was shown to improve the electrochemical properties, especially in the case of nickelate materials [6].

## 2. Experimental

Neodymium oxide ( $\text{Nd}_2\text{O}_3$ , 99.9%, Alfa Aesar) and nickel nitrate hexahydrate ( $\text{Ni}(\text{NO}_3)_2 \cdot 6\text{H}_2\text{O}$ , Sigma–Aldrich) were used as starting powders. Neodymium oxide was first dissolved into a slight excess of nitric acid ( $\text{HNO}_3$ , 68 wt% in water, Prolabo). The neodymium nitrate solution obtained was diluted in distilled water to reach the desired concentration. Nickel nitrate was easily dissolved into distilled water, then both nitrates solutions were mixed together in a stoichiometric amount ( $\text{Nd}:\text{Ni} = 2:1$ ) and the precursor solution was finally introduced into the high-frequency ultrasonic mist generator at room temperature. In order to vary the atomization frequency, two different piezoelectric ceramic transducers have been used, characterized by 2.5 and 1.7 MHz frequencies. A synthetic air (80%  $\text{N}_2$ , 20%  $\text{O}_2$ ) flow rate of  $6 \text{ L min}^{-1}$  was selected to carry the formed aerosol through the 3-zones high temperature furnace. Temperature in the last two zones was fixed at  $700^\circ\text{C}$ ,  $900^\circ\text{C}$  or  $1100^\circ\text{C}$  (the first zone always being set  $50^\circ\text{C}$  lower to avoid too fast evaporation of the solvent and heterogeneous precipitation of the solute). Dry powders are recovered outside the furnace using an electrostatic filter. Further details on the experimental setup can be found in previous publications [15,16].

Cathode inks have been prepared mixing USP  $\text{Nd}_2\text{NiO}_{4+\delta}$  powders (70 wt%) with a terpeneol-based dispersant medium, a commercial solvent (also containing terpeneol) from Dupont and a home-made organic binder using a Dispermat milling system. Ytria-doped ceria (YDC  $\text{Ce}_{0.8}\text{Y}_{0.2}\text{O}_{1.9}$ ) inks were prepared similarly from commercial powder from Praxair. YDC buffer layers were screen-printed on both sides of 8YSZ electrolytes and annealed in air at  $1400^\circ\text{C}$  for 1 h, resulting in 2–3  $\mu\text{m}$  thick porous layers. Cathode layers (20–25  $\mu\text{m}$  thick) were subsequently screen-printed on both sides of YDC-coated 8YSZ and annealed at  $1100^\circ\text{C}$  for 3 h.

Each cell consists of a 100  $\mu\text{m}$  thick dense 8YSZ ( $(\text{ZrO}_2)_{0.92}(\text{Y}_2\text{O}_3)_{0.08}$ ) electrolyte coated on both sides with a 2–3  $\mu\text{m}$  thick YDC buffer layer and a 20–25  $\mu\text{m}$  thick  $\text{Nd}_2\text{NiO}_{4+\delta}$  cathode layer. The only difference between each cell is the cathode microstructure and crystallinity, every other parameter (electrolyte, YDC interlayer, ink composition, screen printing parameters, annealing steps) being identical. Comparisons have been performed using commercial  $\text{Nd}_2\text{NiO}_{4+\delta}$  powders deposited using the same procedure. For relevant comparisons all samples have been processed in conditions optimized for the reference commercial powder.

These symmetrical cells have been characterized by impedance spectroscopy measurements (Autolab PGSTAT 302N coupled with a frequency response analyzer) at open circuit potential in the

frequency range  $10^6$ – $10^{-2}$  Hz (10 points per decade) under air between  $500^\circ\text{C}$  and  $800^\circ\text{C}$ . The magnitude of the measuring sinusoidal voltage was chosen equal to 50 mV to ensure the linearity of the electrical response. Platinum grids (mesh 225) mechanically pressed against both electrodes were used as electrical current collectors. Platinum wires were used to connect electrodes to the external electrical circuit.

The particles morphology and cathode layer microstructure were studied using high resolution scanning electron microscopy (HR-SEM, JEOL 6700) under 5.0 kV accelerated voltage and transmission electron microscopy (TEM JEOL 2000). The particle size was evaluated from the SEM micrographs by counting over 500 particles using Image Tool software; the main particle size reported here corresponds to  $d_{0.5}$  (50% of the particles are below this size). Dilatometric analyses were performed with the help of a Netzsch STA 409 C/CD apparatus under an air flow of  $100 \text{ mL min}^{-1}$  (heating rate  $2 \text{ K min}^{-1}$  from room temperature up to  $1000 \text{ K}$ ). X-ray powder diffraction (XRD) characterization was performed on a PANalytical X'Pert MPD diffractometer in  $\theta$ – $\theta$  configuration with a Cu  $\text{K}\alpha$  radiation ( $\lambda = 1.5418$ ) over the  $2\theta$  range  $5$ – $80^\circ$  in a  $0.036^\circ \text{ s}^{-1}$  continuous scan mode at room temperature.

## 3. Results and discussion

### 3.1. Control of crystallinity, particle size and morphology

Before addressing the electrochemical properties of USP  $\text{Nd}_2\text{NiO}_{4+\delta}$  cathodes, we will first summarize the results previously reported concerning the high control offered by USP over nickelate powder properties; for additional details one can refer to [16]. Control of the primary particle diameter using the process parameters is one of the most important advantages of this synthesis method since it allows fine control of the particle size and crystallinity. Indeed, the reactions responsible for product formation are confined within the individual micrometer-sized droplets which act as individual chemical reactors. The four main operating parameters controlling properties of the final powders are the concentration of the precursor solution, the atomization frequency, the furnace temperature and the carrier gas flow rate. Simply changing one of these four parameters will change the size of the particle, and consequently the primary particle diameter and morphology, as well as its crystallinity [16,17].

Adjusting the precursor solution concentration as well as the atomization frequency allows fine tuning of the particle size. Table 1 presents the experimental parameters for USP synthesis and the corresponding main particle size for each sample. Theoretically, the particle size varies linearly with the droplet size (influenced by atomization frequency) and with the precursor concentration to the power 1/3 as confirmed with our experiments. Fig. 1 provides some examples of morphologies of  $\text{Nd}_2\text{NiO}_{4+\delta}$  USP powders. Comparison between samples 1 (Fig. 1a) and 3 (Fig. 1b) clearly shows the influence of the precursor concentration over particle size; decreasing the concentration from  $5 \times 10^{-2} \text{ M}$  to  $5 \times 10^{-3} \text{ M}$  leads to a reduction in main particle size from 542 nm to 190 nm. Atomization frequency does not only control the particle size but also the particle size distribution (PSD). High atomization frequency (2.5 MHz instead of 1.7 MHz) generates smaller aerosol droplets, reducing the probability of collisions between droplets responsible for the broad particle size distribution usually observed using spray pyrolysis.

The powder morphology varies in regard to the precursor concentration and pyrolysis temperature. Smooth and spherical nanoparticles are synthesized at lower concentrations (Fig. 1b) while rougher particles with more irregular shapes are obtained at higher concentrations (Fig. 1a and c). Surface precipitation becomes

**Table 1**Experimental parameters for the synthesis of USP  $\text{Nd}_2\text{NiO}_{4+\delta}$  powders and  $R_p$  values at 600 °C for the corresponding  $\text{Nd}_2\text{NiO}_{4+\delta}$ /YDC/8YSZ half cells.

	Experimental parameters for USP $\text{Nd}_2\text{NiO}_{4+\delta}$ powder synthesis			Main particle size (nm)	$R_p$ 600 °C ( $\Omega \text{ cm}^2$ )
	Pyrolysis temperature (°C)	Precursor concentration ( $\times 10^{-3} \text{ mol L}^{-1}$ )	Atomization frequency (MHz)		
<b><math>\text{Nd}_2\text{NiO}_{4+\delta}</math>/YDC/8YSZ cells</b>					
1	700	50	1.7	542	8.65
1 annealed 900 °C 1 h	700	–	–	(Sintered grains)	4.08
2	700	50	2.5	463	4.27
3	700	5	1.7	190	4.53
4	900	50	1.7	521	2.59
5	1100	50	2.5	423	1.80
6	1100	50	1.7	474	1.91

significant for large droplet sizes combined with fast evaporation [20] (i.e. for high precursor concentration combined with high pyrolysis temperature) leading to the emergence of open porosity for the larger particles (Fig. 1c).

Finally, powder crystallinity depends on the pyrolysis temperature: amorphous powders are obtained for a moderate temperature (i.e. 700 °C) whereas highly crystalline powders are formed at high pyrolysis temperature (i.e. 1100 °C). XRD pattern representative of  $\text{Nd}_2\text{NiO}_{4+\delta}$  powders synthesized at 1100 °C is shown in Fig. 1d. Because the amorphous powders exhibit high reactivity (calcination of 1 h at 900 °C under air is sufficient to induce  $\text{Nd}_2\text{NiO}_{4+\delta}$  crystallization), the  $\text{Nd}_2\text{NiO}_{4+\delta}$  cathode layer deposited from USP powders is always well crystallized after a short annealing step. It is remarkable to synthesize highly crystalline  $\text{Nd}_2\text{NiO}_{4+\delta}$  powders (average crystallite size =  $35 \pm 3$  nm) with such short reaction times (8 s) while low temperature syntheses [11,13,14,18,19] and solid state reaction [2,13] systematically require a subsequent annealing step (8–12 h) over 1000 °C.

### 3.2. Electrode microstructure

The electrode microstructure has been investigated by SEM. Good adhesion has been observed between the cathode layer and the YDC interlayer (Fig. 2a). Although low particle size can enhance

cracking problems [6], it is worth mentioning that this issue has not been observed with USP powders exhibiting particle size as low as 190 nm. Comparison between Fig. 2b and c proves more advanced sintering for the cathode made from  $\text{Nd}_2\text{NiO}_{4+\delta}$  USP powder than for the cathode made from a commercial powder with  $d_{0.5}$  equal to about 800 nm.

Enhanced sintering of the powders synthesized by USP is also demonstrated by dilatometry measurements shown in Fig. 3. For instance, the sintering of powder 6 begins approximately at a temperature 100 °C lower than for the reference powder. Furthermore, powder densification is much higher for the USP powder ( $dL/L = 236 \times 10^{-3}$  instead of  $124 \times 10^{-3}$  at 1300 °C). The signal derivative also shows multiple sintering steps that could be due to the particle size dispersion, the smaller particles being sintered at lower temperatures than the larger ones. Here particle size distribution and morphology clearly have a role. A narrower particle size distribution (PSD) (enabled by higher atomization frequency) eliminates the scarce larger particles, which leads to much higher sinterability. Powders synthesized with high concentrations and high temperature already underwent plastic deformation and shrinkage during the pyrolysis process which should also be beneficial to the sintering activity. One major benefit of using  $\text{Nd}_2\text{NiO}_{4+\delta}$  powders produced by USP comes from their high reactivity (illustrated by the fast crystallization of  $\text{Nd}_2\text{NiO}_{4+\delta}$  at

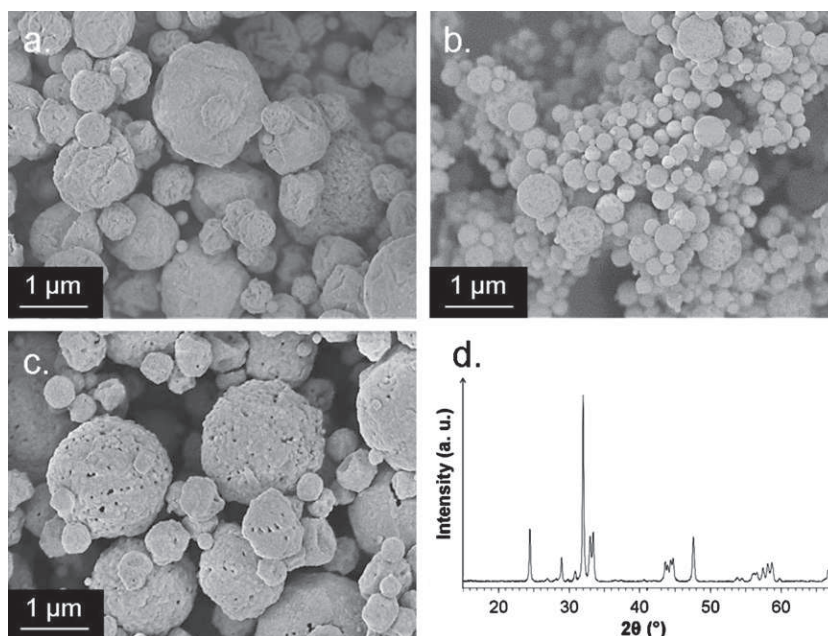


**Fig. 1.** SEM micrographs showing the different particle sizes and morphologies of  $\text{Nd}_2\text{NiO}_{4+\delta}$  powders synthesized by ultrasonic spray pyrolysis: (a) powder 1 ( $T=700$  °C,  $C=5 \times 10^{-2}$  M,  $f=1.7$  MHz), (b) powder 3 ( $T=700$  °C,  $C=5 \times 10^{-3}$  M,  $f=1.7$  MHz) and (c) powder 6 ( $T=1100$  °C,  $C=5 \times 10^{-2}$  M,  $f=1.7$  MHz), (d) X-ray diffraction pattern of powder 6.

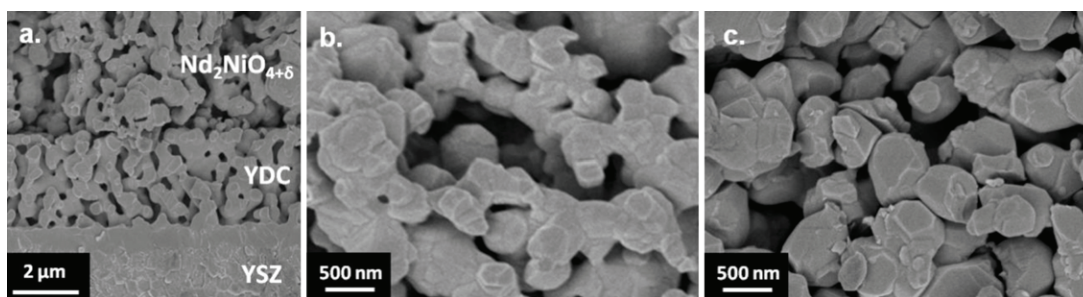


Fig. 2. SEM micrographs of (a) cell 5, (b) cathode layer of cell 5 and (c) cathode layer of reference cell.

moderate temperatures when starting from amorphous powders) inducing high sintering activity. Consequently, this technique offers finer control of the cathode microstructure which could be associated with a reduction in temperature during the annealing step of the cathode layer in an effort to minimize the chemical diffusion at the cathode/buffer layer and buffer layer/electrolyte interfaces.

### 3.3. Electrochemical performances

The influence of the electrode microstructure on the corresponding electrochemical properties of  $\text{Nd}_2\text{NiO}_{4+\delta}$  cathode layers deposited by screen printing has been carefully studied. The electrochemical performances of symmetrical cells made with different USP  $\text{Nd}_2\text{NiO}_{4+\delta}$  powders have been compared with those of a reference cell made with  $\text{Nd}_2\text{NiO}_{4+\delta}$  commercial powder [21]. Therefore the differences observed are discussed in regard to the initial intrinsic properties of the cathode powder (mainly crystallinity and particle size) and the differences in electrode microstructure which can be induced during thermal annealing. Here it is worth noting that the parameters adopted for the cathode layer deposition and subsequent annealing step for all samples in this study have been determined after a lengthy optimization process concerning the reference powder [13]. In order to attribute differences in electrochemical properties solely to the cathode powder used, USP samples have been processed in the same exact conditions.

A typical impedance spectrum obtained is shown in Fig. 4. The experimental diagrams were decomposed by means of a nonlinear least square fit using the Zview2<sup>®</sup> software (Scribner Associates), into two or three elementary contributions (parallel combinations of resistance and constant phase element connected in series), depending on the measuring temperature; the corresponding equivalent circuit is shown in Fig. 4. Hereafter the discussion will

be focused on the results related to the series resistance  $R_s$  and the polarization resistance  $R_p$ . For the sake of comparison, both resistances were normalized by the electrode area. The series resistance was determined by the intercept of the high frequency part of the electrode characteristic on the real axis in the Nyquist plane. The polarization resistance was deduced from the difference between the low frequency real part of the electrode impedance and the series resistance, divided by 2 since symmetrical cells were characterized. Table 1 summarizes the main experimental parameters used for synthesizing the different USP powders used as cathodes layers along with the particle size and  $R_p$  values at 600 °C for the corresponding cells. Fig. 5 presents  $R_p$  values plotted versus  $1000/T$ . Average activation energy is  $1.16 \pm 0.04$  eV which is comparable to the one of the reference cell (1.13 eV).

From the results of Fig. 5, the first peculiar feature is that cathodes made from highly crystalline powders (cells 5 and 6, pyrolysis temperature of 1100 °C) exhibit the lowest polarization resistances, which are closed to values recorded for the reference cell within the experimental accuracy. In situ crystallization of the cathode material on top of the YDC interlayer (starting from amorphous powders as for cells 1–3 with a pyrolysis temperature of 700 °C) leads to poorer results. This is likely to originate from small amounts of impurities (1.0 wt% nitrogen and 0.6 wt% hydrogen as measured by Inductive-Coupled Plasma and CHNS analyzer combined with thermogravimetric analyses [16]) which hinder sintering of amorphous powders and yield lower intimate contacts with YDC. Preliminary heat treatment (900 °C, 1 h under air) of the amorphous cathode powders to induce  $\text{Nd}_2\text{NiO}_{4+\delta}$  crystallization before their screen-printing deposition results in decreased polarization resistance by a factor of 2, which underlines the importance of the initial powder crystallinity. Intermediate  $R_p$  values recorded for cell 4 (pyrolysis temperature of 900 °C) also support this assumption.

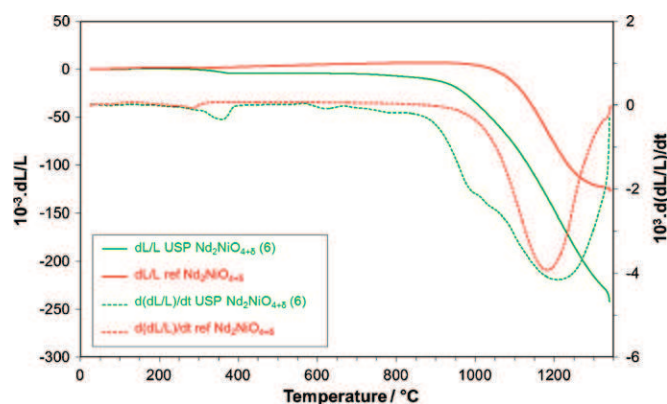


Fig. 3. Dilatometry curves (solid lines) and signal derivative (dotted lines) for USP  $\text{Nd}_2\text{NiO}_{4+\delta}$  powder 6 (green curves) and reference  $\text{Nd}_2\text{NiO}_{4+\delta}$  powder (red curves). (For interpretation of the references to color in this figure legend, the reader is referred to the web version of the article.)

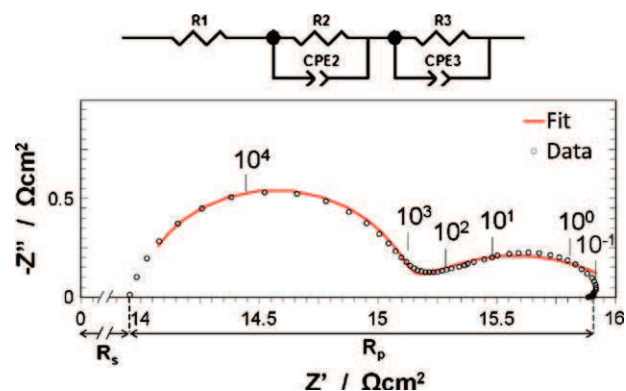


Fig. 4. Typical experimental impedance diagram for  $\text{Nd}_2\text{NiO}_{4+\delta}$ /YDC/YSZ cells (measurement at 600 °C for cell 6). The corresponding equivalent circuit used for fitting is also displayed, the fitting curve is overlaid on the data points and signal frequency is indicated.

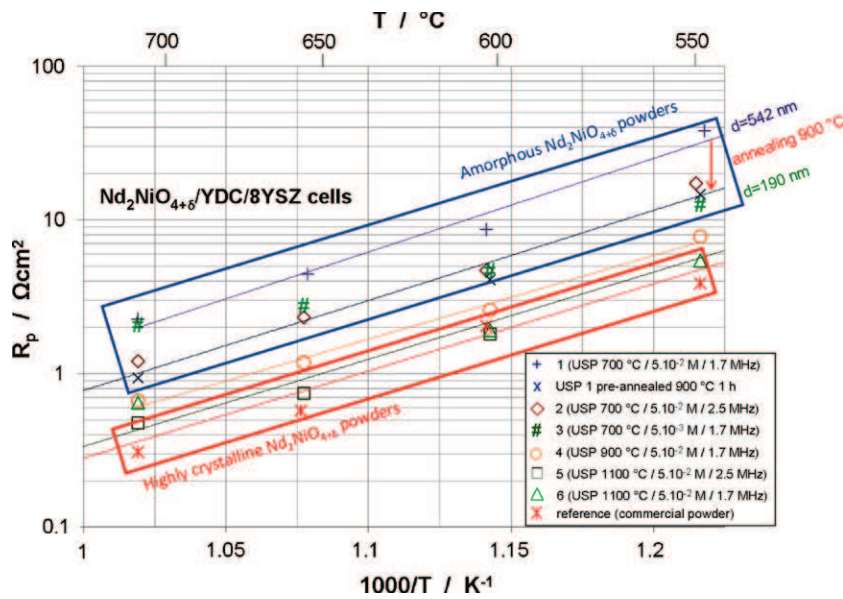


Fig. 5. Arrhenius plot of polarization resistance ( $R_p$ ) for  $\text{Nd}_2\text{NiO}_{4+\delta}$ /YDC/YSZ cells with different  $\text{Nd}_2\text{NiO}_{4+\delta}$  cathode layers. Experimental parameters for USP  $\text{Nd}_2\text{NiO}_{4+\delta}$  powders used in cells 1–6 are indicated (pyrolysis temperature, precursor concentration and atomization frequency, respectively).

The second feature to underline is that smaller particle size and narrower PSD (for instance, by increasing the atomization frequency) are beneficial for the electrochemical properties of cathode, particularly for the ones made from amorphous powders since the rare very large micron-sized particles are mostly responsible for the organic impurity release during the sintering step. Indeed impedance spectroscopy measurement for cells 1 and 3 show that lower particle size (542 nm and 190 nm respectively, with precursor concentration divided by 10) leads to a significant decrease of  $R_p$  ( $8.65 \Omega \text{ cm}^2$  and  $4.53 \Omega \text{ cm}^2$  respectively). The change induced by a narrower PSD for highly crystalline powders is less noticeable since the microstructure is still more regular. The closed polarization resistances of cells 5 and 6 (particle size lower than 500 nm) and the reference one (particle size of

800 nm) could be regarded as conflicting. But, the sintering activity of USP  $\text{Nd}_2\text{NiO}_{4+\delta}$  is higher (Fig. 3) and a lower mean porosity after sintering can thus impede the access of the gas phase to the reaction sites. At this stage, it is worth noting that, without any optimization of the processing parameters, the  $R_p$  values reported here are already remarkably low, i.e. less than  $0.3 \Omega \text{ cm}^2$  at 700 °C which compares favorably with the  $0.5 \Omega \text{ cm}^2$  value cited in introduction.

Similar trends can be extracted from the variation of the series resistance as a function of the powder crystallinity of the cathode layer (Fig. 6). The higher is the crystallinity, the lower the series resistance. This confirms that an enhanced sintering of  $\text{Nd}_2\text{NiO}_{4+\delta}$  yields better contacts with the YDC interlayer. Moreover, for a given crystallinity, the influence of the particle size on the series

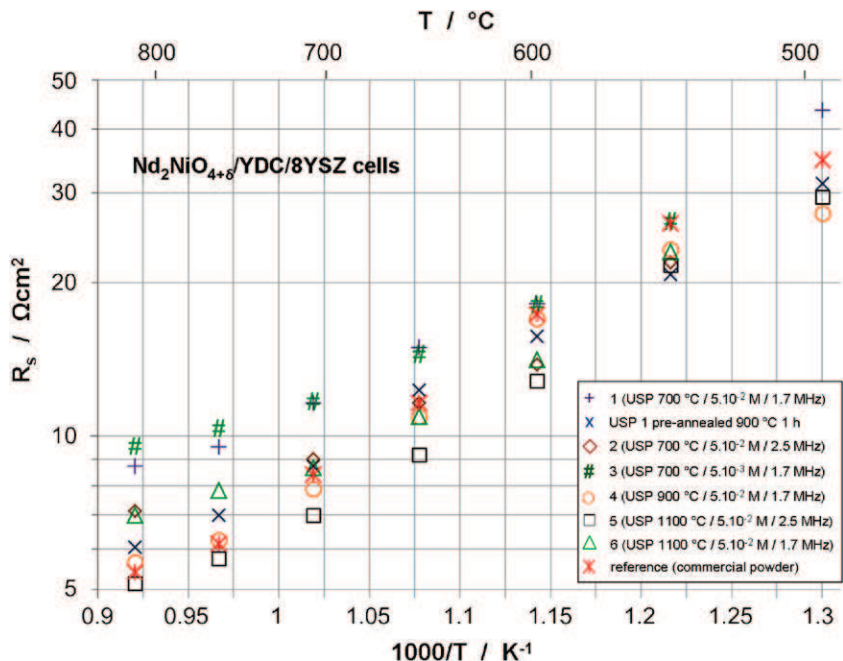


Fig. 6. Arrhenius plot of series resistance ( $R_s$ ) for  $\text{Nd}_2\text{NiO}_{4+\delta}$ /YDC/YSZ cells with different  $\text{Nd}_2\text{NiO}_{4+\delta}$  cathode layers.

resistance is far less pronounced than for the polarization resistances. This indicates that the respective volumes related to each resistive contribution are different, as could be expected for a MIEC electrode. It is worth noting that the experimental values of  $R_s$  are higher than those which can be calculated from the conductivities of YSZ [22] and YDC [23] and the related volumes. This suggests that the series resistance includes the contribution of constriction of current lines related to an insufficient current collection which can strongly alter the performance of a SOFC cathode [24,25]. Indeed, the sheet resistance arising from the electron transport within the cathode layer is expected to be negligible since the electronic conductivity of  $\text{Nd}_2\text{NiO}_{4+\delta}$  is higher than  $10\text{Scm}^{-1}$  [2]. In this study, one cannot distinguish the relative contributions of the  $\text{Nd}_2\text{NiO}_{4+\delta}$ /YDC and  $\text{Nd}_2\text{NiO}_{4+\delta}$ /current collector interfaces to the current constriction effect.

#### 4. Conclusions

This study is the first assessment of the suitability of the USP technique, offering great opportunities to tune the powder properties in particular powder crystallinity and particle size, for an SOFC application. The aim of this paper was to show the relationships between the cathode powder properties and the cathode resistance to identify experimental parameters leading to best results in terms of electrochemical performance. Electrochemical impedance spectroscopy measurements show that the series resistance  $R_s$  and the polarization resistance  $R_p$  are both dependent on the microstructure of the electrode and exhibit the same variation trends. The best results ( $R_p$  values below  $0.5\ \Omega\ \text{cm}^2$  at  $700\ ^\circ\text{C}$  and  $2\ \Omega\ \text{cm}^2$  at  $600\ ^\circ\text{C}$ ) are obtained from highly crystalline USP powders with low particle size (about 400 nm). Finally, highly reactive powders exhibit a significantly improved sintering activity which leads to a different electrode microstructure than the reference cell, show a good adhesion of the cathode layer and contribute to the lowering of the cathode resistance. While this study demonstrates the potential of USP  $\text{Nd}_2\text{NiO}_{4+\delta}$  powders, electrochemical performances of USP powders could be again enhanced after an optimization of the processing parameters (especially the sintering step owing to their reactivity much higher than the one of the reference powder). Following these results which demonstrated the interest of spray pyrolysis synthesis for SOFCs materials, another project currently under way focuses on the USP synthesis of  $\text{Pr}_2\text{NiO}_{4+\delta}$  powders

which have shown highly promising electrochemical performances at  $600\ ^\circ\text{C}$  [6].

#### Acknowledgment

Financial support from the EC within the integrated project SOFC600 (Contract No. 020089) is gratefully acknowledged.

#### References

- [1] E. Boehm, J.-M. Bassat, M.C. Steil, P. Dordor, F. Mauvy, J.-C. Grenier, *Solid State Sciences* 5 (2003) 973.
- [2] E. Boehm, J.-M. Bassat, P. Dordor, F. Mauvy, J.-C. Grenier, P. Stevens, *Solid State Ionics* 176 (2005) 2717.
- [3] J.A. Kilner, C.K.M. Shaw, *Solid State Ionics* 154–155 (2002) 523.
- [4] V.V. Vashook, L.L. Yushkevich, L.V. Kokhanovsky, L.V. Makhnach, S.P. Tolochko, I.F. Kononyuk, H. Ullmann, H. Altenburg, *Solid State Ionics* 119 (1999) 23.
- [5] D.C. Zhu, X.Y. Xu, S.J. Feng, W. Liu, C.S. Chen, *Catalysis Today* 82 (2003) 151.
- [6] C. Ferchaud, J.-C. Grenier, Y. Zhang-Steenwinkel, M.M. van Tuel, F.P. van Berkel, J.-M. Bassat, *Journal of Power Sources* 196 (2011) 1872.
- [7] J.-M. Bassat, P. Odier, A. Villesuzanne, C. Marin, M. Pouchard, *Solid State Ionics* 167 (2004) 341.
- [8] M. Burriel, G. Garcia, J. Santiso, J.A. Kilner, R.J. Chater, S.J. Skinner, *Journal of Materials Chemistry* 18 (2008) 416.
- [9] R. Sayers, R. De Souza, J. Kilner, S. Skinner, *Solid State Ionics* 181 (2010) 386.
- [10] J.-M. Bassat, M. Petitjean, J. Fouletier, C. Lalanne, G. Caboche, F. Mauvy, J.-C. Grenier, *Applied Catalysis A* 289 (2005) 84.
- [11] C. Lalanne, G. Prosperi, J.-M. Bassat, F. Mauvy, S. Fourcade, P. Stevens, M. Zahid, S. Diethelm, J. Van Herle, J.-C. Grenier, *Journal of Power Sources* 185 (2008) 1218.
- [12] C. Lalanne, F. Mauvy, J.-M. Bassat, J.-C. Grenier, D. Pordor, M. Pouchard, in: M. Mogensen (Ed.), *Proc. 6th Europ. SOFC, 2004*, ISBN 3-905592-15-0, p. 1351.
- [13] C. Lalanne, F. Mauvy, E. Siebert, M. Fontaine, J.-M. Bassat, F. Ansart, P. Stevens, J.-C. Grenier, *Journal of the European Ceramic Society* 27 (2007) 4195.
- [14] F. Mauvy, C. Lalanne, J.-M. Bassat, J.-C. Grenier, H. Zhao, P. Dordor, P. Stevens, *Journal of the European Ceramic Society* 25 (2005) 2669.
- [15] R. Rocha, E. Muccillo, L. Dessemond, E. Djurado, *Journal of the European Ceramic Society* 30 (2010) 227.
- [16] D. Mesguich, J.-M. Bassat, C. Aymonier, E. Djurado, *Solid State Ionics* 181 (2010) 1015.
- [17] E. Djurado, E. Meunier, *Journal of Solid State Chemistry* 141 (1998) 191.
- [18] G. Amow, S. Skinner, *Journal of Solid State Electrochemistry* 10 (2006) 538.
- [19] J. Wan, J. Goodenough, J. Zhu, *Solid State Ionics* 178 (2007) 281.
- [20] G.L. Messing, S.-C. Zhang, G.V. Jayanthi, *Journal of the American Ceramic Society* 76 (1993) 2707.
- [21] <http://www.mariontechnologies.com/nanomateriaux/english/material.html>
- [22] Project EVERESTE, Contract No. ANR-07-PANH-005.
- [23] S. Li, L. Ge, H. Gu, Y. Zheng, H. Chen, L. Guo, *Journal of Alloys and Compounds* 509 (2011) 94.
- [24] K. Sasaki, J.-P. Wurth, R. Gschwend, M. Godickemeier, L.J. Gauckler, *Journal of the Electrochemical Society* 143 (1996) 530.
- [25] S.P. Jiang, J.G. Love, L. Apateanu, *Solid State Ionics* 160 (2003) 15.